Embedded Pilot-Aided Channel Estimation for OTFS in Delay–Doppler Channels

P. Raviteja, *Student Member, IEEE*, Khoa T. Phan, *Member, IEEE*, and Yi Hong, *Senior Member, IEEE*

***Abstract*—Orthogonal time frequency space (OTFS) modulation was shown to provide significant error performance advantages over orthogonal frequency division multiplexing (OFDM) in delay–Doppler channels. In order to detect OTFS modulated data, the channel impulse response needs to be known at the receiver. In this paper, we propose embedded pilot-aided channel estimation schemes for OTFS. In each OTFS frame, we arrange pilot, guard, and data symbols in the delay–Doppler plane to suitably avoid interference between pilot and data symbols at the receiver. We develop such symbol arrangements for OTFS over multipath channels with integer and fractional Doppler shifts, respectively. At the receiver, channel estimation is performed based on a threshold method and the estimated channel information is used for data detection via a message passing algorithm. Thanks to our specific embedded symbol arrangements, both channel estimation and data detection are performed within the same OTFS frame with minimum overhead. We compare through simulations the error performance of OTFS using the proposed channel estimation and OTFS with ideally known channel information and observe only a marginal performance loss. We also demonstrate that the proposed channel estimation in OTFS significantly outperforms OFDM with known channel information. Finally, we present extensions of the proposed schemes to multiple-input multiple-output (MIMO) and multi-user uplink/downlink.**

***Index Terms*—OTFS, delay–Doppler channel, channel estimation, pilot arrangement.**

I. Introduction

ORTHOGONAL frequency division multiplexing (OFDM) is a popular modulation scheme that is currently deployed in 4G long term evolution (LTE) mobile systems. OFDM is known to achieve good robustness and high spectral efficiency for time-invariant frequency selective channels. However, for high-mobility environments such as high-speed railway mobile communications, the channels can be typically time-varying with high Doppler spreads. Under such high Doppler conditions, OFDM is no longer robust and suffers heavy performance degradations. Hence, new modulation schemes that are robust to channel time-variations are being extensively explored.

Manuscript received August 24, 2018; revised December 26, 2018 and February 13, 2019; accepted March 16, 2019. Date of publication March 20, 2019; date of current version May 28, 2019. This work was supported by the Australian Research Council through the Discovery Project under Grant DP160100528. The review of this paper was coordinated by Prof. Y. T. Su. *(Corresponding author: Yi Hong.)*

P. Raviteja and Y. Hong are with the ECSE Department, Monash University, Clayton, VIC 3800, Australia (e-mail: raviteja.patchava@monash.edu; yi.hong@monash.edu).

K. T. Phan is with the CSIT Department, La Trobe University, Bendigo, VIC 3550, Australia (e-mail: k.phan@latrobe.edu.au).

Digital Object Identifier 10.1109/TVT.2019.2906357

Recently, orthogonal time frequency space (OTFS) modulation was proposed in [1], [2]. OTFS exhibits significant advantages over OFDM in multipath delay–Doppler channels where each path exhibits a different delay and Doppler shift. In particular, the idea of transmission in the delay-Doppler domain was introduced in [1], [2]. The delay–Doppler domain provides as an alternative representation of a time-varying channel geometry due to moving objects (e.g. transmitters, receivers, or reflectors) in the scene. Leveraging on this representation, OTFS multiplexes each information symbol over a two dimensional (2D) orthogonal basis functions, specifically designed to combat the dynamics of time-varying multipath channels. Then the information symbols placed in the delay-Doppler coordinate system can be converted to the standard time-frequency domain used by traditional modulation schemes such as OFDM. More recently, in [13], a simplified OTFS structure was proposed by including OFDM for time-frequency signal modulation. Its extension to the multiple-input multiple-output (MIMO) case was presented in [14].

In general, OTFS uses the delay-Doppler channel response [1]–[3] to parameterize the effects of a time-varying channel on any transmitted waveform. In the delay-Doppler domain, the response captures the dominant scatterers in the channel, with their specific delay and Doppler parameters. In the time-frequency domain, this corresponds to a standard time-varying impulse response.

Estimating delay-Doppler channel response at the receiver is necessary to perform OTFS detection [4]–[12]. Hence, in [11], [12], [15], [16], pilot-aided channel estimation techniques were investigated.

In [12], an entire OTFS frame was used for pilot transmission and the estimated channel information was used for data detection in next frame. This method may not be effective if the channel estimation becomes outdated in the following frame. In [11], [16], OTFS channel estimation was conducted in the time–frequency domain, resulting in higher implementation complexity than that of [12], [15], where the channel estimation was conducted in delay–Doppler domain. In [15], pilot-aided channel estimation was considered for OTFS with ideal pulse-shaping waveform over channels with integer Doppler shifts only, i.e., when the channel Doppler taps are aligned to integer delay–Doppler grid. Further, the exact symbol deployment and channel estimation technique are not described in [15].

Motivated by the pilot-aided channel estimation idea in [15], in this paper, we consider multipath channels with integer and

fractional Doppler shifts, respectively.[1] Under such setting, we propose an embedded OTFS channel estimation scheme for point-to-point single-input single-output (SISO) system with ideal and rectangular pulse-shaping waveforms, respectively. Specifically, for each OTFS frame, we arrange a single pilot symbol, guard symbols, and data symbols in the delay–Doppler grid to suitably avoid the interference between pilot and data symbols. At the receiver, channel estimation is performed based on a threshold method and the estimated channel information is used for data detection via a message passing (MP) algorithm in [4]. Depending on the channel and symbol arrangement, the threshold is chosen to optimize the estimation accuracy. Thanks to our specific embedded symbol arrangements, both channel estimation and data detection are performed within the same OTFS frame with a minimum overhead (1% for integer Doppler case and 8% for fractional Doppler case).[2]

We compare by simulations the performance of OTFS using the proposed channel estimation schemes and OTFS with perfectly known channel information and observe only a marginal performance degradation. Further, we show that OTFS with our channel estimation significantly outperforms OFDM, with known channel information.

Finally, we present the extensions of the proposed channel estimation schemes to MIMO and multi-user uplink/downlink.

The rest of the paper is organized as follows. Section II reviews basic OTFS concepts and results, which lay the foundations for the development of OTFS-based channel estimation schemes in Section III. Numerical results are presented in Section IV. Extensions of the proposed channel estimation schemes with pilot, guard, and data symbols arrangement to MIMO and multiuser OTFS systems are presented in Section V followed by the conclusions in Section VI.

II. OTFS: Basic Concepts and Results

In this section, we first review the basic concepts and results of OTFS from [1], [2], [4].

A. Basic OTFS Concepts/Notations

– The *time–frequency signal plane* is discretized to a $M \times N$ grid (for some integers $N, M > 0$) by sampling time and frequency axes at intervals T (seconds) and Δf (Hz), respectively, i.e.,

$$\Lambda = \big\{(nT, m\Delta f),\ n = 0, \ldots, N-1, m = 0, \ldots, M-1\big\}$$

– The modulated *time–frequency samples* $X[n,m], n = 0, \ldots, N-1, m = 0, \ldots, M-1$, are transmitted over an OTFS frame with duration $T_f = NT$ and bandwidth $B = M\Delta f$.

[1]Fractional Doppler shifts usually occur with a low Doppler resolution.

[2]It should be noted that a joint channel estimation and data detection scheme can also fit the MP algorithm and possibly improve the error performance due to imperfect channel estimation. This is an interesting future research topic.

– The delay–Doppler plane is discretized to a $M \times N$ *information* grid

$$\Gamma = \left\{\left(\frac{k}{NT}, \frac{l}{M\Delta f}\right),\ k = 0, \ldots, N-1, l = 0, \ldots, M-1\right\},$$

where $1/M\Delta f$ and $1/NT$ represent the quantization steps of the delay and Doppler frequency axes, respectively.

B. OTFS Mod/Demod

The modulator first maps a set of NM information symbols $\{x[k,l], k = 0, \ldots, N-1, l = 0, \ldots, M-1\}$ from a modulation alphabet $\mathbb{A} = \{a_1, \cdots, a_Q\}$ (e.g. QAM symbols) of size Q, arranged on the delay–Doppler information grid Γ, to $X[n,m]$ in the time–frequency domain grid using the *inverse symplectic finite Fourier transform* (ISFFT). Next, the *Heisenberg transform* is applied to $X[n,m]$ using transmit pulse $g_{\rm tx}(t)$ to create the time-domain signal $s(t)$.

The signal $s(t)$ is then transmitted over the wireless channel with complex baseband channel impulse response $h(\tau, \nu)$, which characterizes the channel response to an impulse with delay τ and Doppler ν [18]. The received signal $r(t)$ is processed with the *Wigner transform* (implementing a receiver filter with an impulse response $g_{\rm rx}(t)$) followed by a sampler, yielding $Y[n,m]$ in the time–frequency domain. We then apply SFFT on $Y[n,m]$ to obtain received symbols $y[k,l]$ in the delay–Doppler domain for symbol detection [1].

C. OTFS Input–Output Analysis

We now look at the relations between received symbols $y[k,l]$ and transmitted symbols $x[k,l]$.

We assume that $h(\tau, \nu)$ has finite support bounded by $[0, \tau_{\max}]$ on the delay axis and $[-\nu_{\max}, \nu_{\max}]$ on the Doppler axis, where $\tau_{\max}$ and $\nu_{\max}$ are the maximum delay and the maximum Doppler shift among all channel paths. Since typically there are only a small number of reflectors in the channel with associated delays and Dopplers, very few parameters are needed to model the channel in the delay-Doppler domain. The sparse representation of the channel is

$$h(\tau, \nu) = \sum_{i=1}^{P} h_i \delta(\tau - \tau_i)\delta(\nu - \nu_i)$$

where P is the number of propagation paths, h_i, τ_i, and ν_i represent the complex gain, delay, and Doppler shift associated with the i-th path, and $\delta(\cdot)$ denotes the Dirac delta function. We denote by l_{τ_i}, k_{ν_i} the delay and Doppler *taps* for the i-th path (relatively to the delay–Doppler grid Γ) defined as

$$\tau_i = \frac{l_{\tau_i}}{M\Delta f},\quad \nu_i = \frac{k_{\nu_i} + \kappa_{\nu_i}}{NT} \tag{1}$$

where $-\frac{1}{2} < \kappa_{\nu_i} \leq \frac{1}{2}$ represents the *fractional Doppler*, i.e., the fractional shift from the nearest Doppler tap k_{ν_i}. We do not need to consider fractional delays, since the resolution $1/M\Delta f$ of the time axis is sufficient to approximate the path delays to the nearest sampling points in typical wide-band systems [20]. Let

us denote l_τ and k_ν the delay and Doppler taps corresponding to the largest delay $\tau_{\max}$ and Doppler $\nu_{\max}$.

We also assume that the pulses $g_{\text{tx}}(t)$ and $g_{\text{rx}}(t)$ are *ideal*, meaning that they satisfy the *bi-orthogonal property* condition [1], i.e., the *cross-ambiguity function* $A_{g_{\text{rx}},g_{\text{tx}}}(t,f)=0$ for $t\in(nT-\tau_{\max},nT+\tau_{\max})$, $f\in(m\Delta f-\nu_{\max},m\Delta f+\nu_{\max})$, $\forall n,m$, except for $n=0,m=0$, where $A_{g_{\text{rx}},g_{\text{tx}}}(t,f)=1$ with $t\in(-\tau_{\max},\tau_{\max})$ and $f\in(-\nu_{\max},+\nu_{\max})$. The case of non-ideal yet practical rectangular pulses is discussed in Section III.

1) Integer Doppler shifts: The relation between $y[k,l]$ and $x[k,l]$ was derived in [4] as

$$y[k,l]=\sum_{k'=-k_\nu}^{k_\nu}\sum_{l'=0}^{l_\tau}b[k',l']\hat{h}[k',l']x[[k-k']_N,[l-l']_M]+v[k,l] \tag{2}$$

where $\hat{h}[k',l']=h[k',l']e^{-j2\pi\frac{k'}{NT}\frac{l'}{M\Delta f}}$, $b[k',l']\in\{0,1\}$ is the path indicator, i.e., $b[k',l']=1$ indicates that there is a path with Doppler tap k' and delay tap l' with corresponding path magnitude $\hat{h}[k',l']$, otherwise, there is no such path, i.e., $b[k',l']=0$ and $\hat{h}[k',l']=0$. Finally, the term $v[k,l]\sim\mathcal{CN}(0,\sigma^2)$ is an additive white noise with variance σ^2, and $[\cdot]_N,[\cdot]_M$ denote modulo N and M operations, respectively. We have the total number of paths:

$$\sum_{k'=-k_\nu}^{k_\nu}\sum_{l'=0}^{l_\tau}b[k',l']=P.$$

Each path circularly shifts the transmitted symbols by the delay and Doppler taps.

2) Fractional Doppler shifts: Similarly, the following result was derived in [4] for the fractional Doppler case

$$y[k,l]=\sum_{k'=-k_\nu}^{k_\nu}\sum_{l'=0}^{l_\tau}b[k',l']\sum_{q=-N/2}^{N/2-1}\bar{h}[k',l',\kappa',q]\,x\left[[k-k'+q]_N,[l-l']_M\right]+v[k,l] \tag{3}$$

where κ' denotes the fractional Doppler associated with the (k',l') path, with the path gain [5, Eq. (20)]

$$\begin{aligned}\bar{h}[k',l',\kappa',q]&=\left(\frac{e^{j2\pi(-q-\kappa')}-1}{Ne^{j\frac{2\pi}{N}(-q-\kappa')}-N}\right)h[k',l']e^{-j2\pi\frac{k'+\kappa'}{NT}\frac{l'}{M\Delta f}}\\&=\alpha(q,\kappa')h[k',l']e^{-j2\pi\frac{k'+\kappa'}{NT}\frac{l'}{M\Delta f}}\end{aligned} \tag{4}$$

where $\alpha(q,\kappa')=(\frac{e^{j2\pi(-q-\kappa')}-1}{Ne^{j\frac{2\pi}{N}(-q-\kappa')}-N})$. The amplitude of $\alpha(q,\kappa')$, $|\alpha(q,\kappa')|$, reduces as q moves further away from 0, since it is equivalent to the sampled version of the Dirichlet sinc function. For illustration, Fig. 2 shows $|\alpha(q,\kappa')|$ as a function of q for $N=128$ and $\kappa'=0.1,0.5$. It can be observed that $|\alpha(q,\kappa')|$ reduces by -15 to -20 dB around $q=-10,10$. The value $q=-10,10$ will be used for the channel approximation purpose in later sections.

It should be noted that a smoother window function can cause $|\alpha(q,\kappa')|$ to decay much faster than the rectangular window function thus reducing the channel approximation error (see (12)). However, implementing a window other than the rectangular function at the receiver results in an correlated noise. Further, whitening the noise affects the sparse structure of OTFS thus increasing the receiver complexity. The study on the effect of a transmitter window is beyond the scope of this paper.

It can also be seen that with fractional Doppler shifts, each received symbol is affected by more transmitted symbols than in the case of integer Doppler in (2). We can see from (3) that when $\kappa'=0$, (3) simplifies to (2) as expected.

D. OTFS Data Detection via Message Passing (MP)

From the received symbols $y[k,l]$, if the channel parameters are known, we can employ the message passing (MP) algorithm in [4] to detect the data symbols $x[k,l]$ using the set of MN linear equations (2) or (3).

III. Embedded Channel Estimation for Point-to-Point SISO Case

We first assume OTFS with ideal waveforms for multipath channel with integer and fractional Doppler cases. Then we consider the extension to OTFS with practical rectangular waveforms.

A. Integer Doppler Case

Let x_p denote the pilot symbol with a *pilot SNR*: $\text{SNR}_p=|x_p|^2/\sigma^2$. Let x_d denote the data symbols with *data SNR* of $\text{SNR}_d=\mathbb{E}(|x_d|^2)/\sigma^2$, in the delay–Doppler information grid, and 0 denote the guard symbol.

Motivated by [15], we place one pilot symbol x_p, N_n of the 0 guard symbols, and $MN-N_n-1$ information symbols in the delay–Doppler grid Γ for each OTFS frame transmission. The symbols are located in such a way so that at the receiver, we can separate two distinct groups of received symbols: the first group that involves pilot and guard symbols is used for channel estimation, and the second group for data detection. Moreover, the guard symbols guarantee that the received symbols for channel estimation and data detection do not interfere with each other. This helps to provide a more accurate channel estimation to be used for data detection within the same frame.

For a pilot, we first choose arbitrary grid location $[k_p,l_p]$ such that $0\le k_p\le N-1$, and $0\le l_p\le M-1$. For ease of representation, we choose $0\le l_p-l_\tau\le l_p\le l_p+l_\tau\le M-1$, and $0\le k_p-2k_\nu\le k_p\le k_p+2k_\nu\le N-1$. Recall that l_τ and k_ν denote the taps corresponding to the maximum delay and Doppler values.

We arrange the pilot, guard, and data symbols in the delay–Doppler grid for an OTFS frame transmission as in Fig. 1a:

$$x[k,l]=\begin{cases}x_p & k=k_p,l=l_p,\\ 0 & k_p-2k_\nu\le k\le k_p+2k_\nu,\\ & l_p-l_\tau\le l\le l_p+l_\tau,\\ x_d[k,l] & \text{otherwise.}\end{cases} \tag{5}$$

In this case, we have $N_n=(2l_\tau+1)(4k_\nu+1)-1$ guard symbols. Using the proposed channel estimation scheme, we can see that the overhead for pilot and guard symbols, $\frac{N_n+1}{MN}$, tends

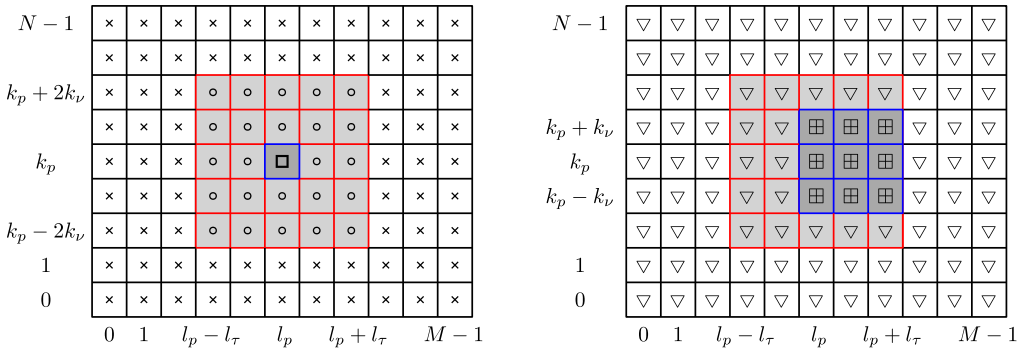

(a) Tx symbol arrangement (□: pilot; ○: guard symbols; ×: data symbols)

(b) Rx symbol pattern (▽: data detection, ⊞: channel estimation)

Fig. 1. The integer Doppler case.

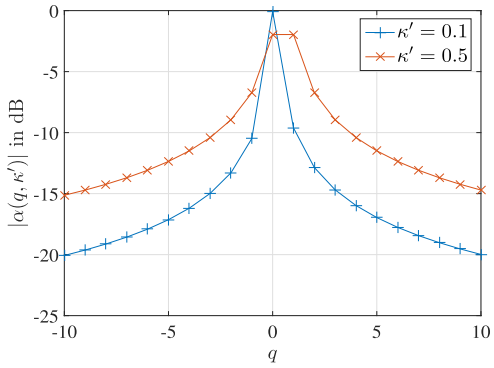

Fig. 2. $|\alpha(q,\kappa')|$ as function of q for $N=128$ and $\kappa'=0.1, 0.5$.

to be small for typical channel models. For example, for Long-Term Evolution (LTE) channels with $l_\tau=20$, $k_\nu=4$, the overhead is approximately 1% of the data frame with $M=512$, and $N=128$ [17].

At the receiver, we use the received symbols $y[k,l], k_p-k_\nu \le k \le k_p+k_\nu, l_p \le l \le l_p+l_\tau$ for channel estimation. Then the remaining received symbols $y[k,l]$ on the grid are used for data detection, as shown in Fig. 1b.

Due to the transmit symbol arrangement in (5), using (2), we can express the received symbols for channel estimation as

$$y[k,l]=b[k-k_p,l-l_p]\hat{h}[k-k_p,l-l_p]x_p+v[k,l]. \quad (6)$$

for $k\in[k_p-k_\nu,k_p+k_\nu], l\in[l_p,l_p+l_\tau]$. We can see that if there is a path with Doppler tap $k-k_p$ and delay tap $l-l_p$, i.e., $b[k-k_p,l-l_p]=1$, we have $y[k,l]=\hat{h}[k-k_p,l-l_p]x_p+v[k,l]$. Otherwise, $y[k,l]=v[k,l]$.

Similarly, we can express the received symbols for data detection as in (2), demonstrating no interference between the received symbols for channel estimation and data detection.

We propose a simple channel estimation algorithm as follows. For $k\in[k_p-k_\nu,k_p+k_\nu], l\in[l_p,l_p+l_\tau]$, if the magnitude $|y[k,l]|\ge\mathcal{T}$, where $\mathcal{T}$ is some positive detection threshold, then we estimate $b[k-k_p,l-l_p]=1$ and $\hat{h}[k-k_p,l-l_p]=y[k,l]/x_p$. Otherwise, we set $b[k-k_p,l-l_p]=\hat{h}[k-k_p,l-l_p]=0$. The proposed threshold-based scheme relies on the fact that if a path exists, the received symbol is the scaled pilot signal with additive white Gaussian noise (see (6)). Otherwise, it is only noise.

By varying the threshold $\mathcal{T}$, we can alter the miss detection or false alarm probabilities on path detection. As a result, the error performance of data detection is affected by $\mathcal{T}$, as will be shown in Section IV.

We then use the estimated information for data detection, i.e., the received symbols $y[k,l]$ for data detection are

$$y[k,l]=\sum_{k'=-k_\nu}^{k_\nu}\sum_{l'=0}^{l_\tau} b[k',l']\hat{h}[k',l']x_d[[k-k']_N,\ [l-l']_M] + v[k,l] \quad (7)$$

for $k\notin[k_p-k_\nu,k_p+k_\nu]$ or $l\notin[l_p,l_p+l_\tau]$. Note that we have a total of $MN-(2k_\nu+1)(l_\tau+1)$ received symbols to detect a smaller number of $MN-(2l_\tau+1)(4k_\nu+1)$ data symbols via the MP algorithm in [4].

B. The Fractional Doppler Case

We consider two cases using full guard symbols and reduced guard symbols, respectively. The former case offers better channel estimation at the expense of the lower spectral efficiency by using more guard symbols and less data symbols, in contrast to the latter case.

1) The Case With Full Guard Symbols: We arrange the pilot, guard, and data symbols in the delay–Doppler grid, as depicted in Fig. 3a:

$$x[k,l]=\begin{cases} x_p, & k=k_p, l=l_p \\ 0, & 0\le k\le N-1, l_p-l_\tau\le l\le l_p+l_\tau \\ x_d[k,l], & \text{otherwise.}\end{cases} \quad (8)$$

For simplicity of notation, we choose $0\le l_p-l_\tau\le l_p\le l_p+l_\tau\le M-1$. We have the number of guard symbols $N_n=(2l_\tau+1)N-1$, and the overhead for pilot and guard symbols is about 8% in the exemple LTE channels described earlier [17].

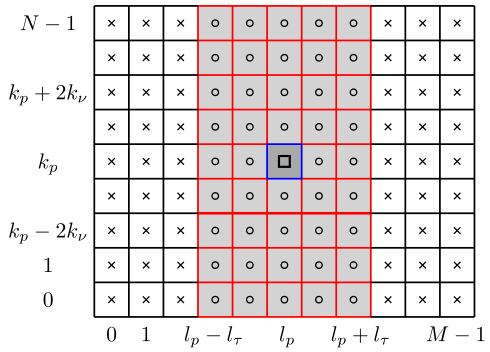

(a) Tx symbol arrangement (□: pilot; ∘: guard symbols; ×: data symbols)

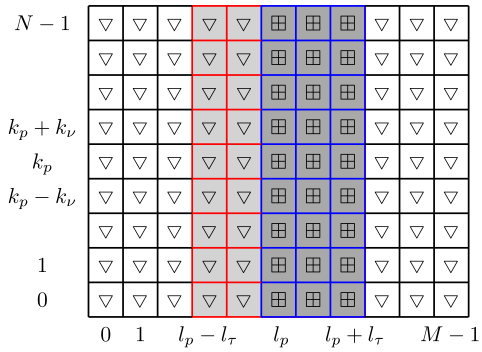

(b) Rx symbol pattern (▽: data detection, ⊞: channel estimation)

Fig. 3. The fractional Doppler case: Full guard symbols.

At the receiver, we use the received symbols $y[k,l], 0 \le k \le N-1, l_p \le l \le l_p + l_\tau$ for channel estimation, and the remaining received symbols $y[k,l]$ for data detection (see Fig. 3b).

Using (3), the received symbols $y[k,l]$ for channel estimation are

$$y[k,l] = \sum_{k'=-k_\nu}^{k_\nu} b[k', l-l_p]\bar{h}[k', l-l_p, \kappa', [k_p+k'-k]_N]\, x_p + v[k,l]$$

for $k \in [0, N-1], l \in [l_p, l_p + l_\tau]$. We can rewrite $y[k,l]$ as

$$y[k,l] = \tilde{b}[l-l_p]\tilde{h}[[k-k_p]_N, l-l_p]x_p + v[k,l] \quad (9)$$

where

$$\tilde{b}[l-l_p] = \begin{cases} 1, & \sum_{k'=-k_\nu}^{k_\nu} b[k', l-l_p] \ge 1 \\ 0, & \text{otherwise} \end{cases}$$

is the path indicator, and

$$\tilde{h}[[k-k_p]_N, l-l_p] = \sum_{k'=-k_\nu}^{k_\nu} b[k', l-l_p]\bar{h}[k', l-l_p, \kappa', [k_p+k'-k]_N]$$

is the effective path gain from the pilot symbol x_p at location $[k_p, l_p]$ to the received symbol $y[k,l]$. Then $\tilde{b}[l-l_p] = 1$ indicates that there is at least one path with delay tap $l - l_p$, otherwise, $\tilde{b}[l-l_p] = 0$.

Based on (9), we propose the following threshold-based channel estimation algorithm.

For $k \in [0, N-1], l \in [l_p, l_p + l_\tau]$, if $|y[k,l]| \ge \mathcal{T}$, then we have $\tilde{b}[l-l_p] = 1$, and $\tilde{h}[[k-k_p]_N, l-l_p] = y[k,l]/x_p$. Otherwise, we set $\tilde{b}[l-l_p] = \tilde{h}[[k-k_p]_N, l-l_p] = 0$. Unlike the integer Doppler case, where we estimate whether an individual path with given delay and Doppler taps exists, in this case, we estimate whether there exists *at least* one path with a given delay tap. That is, if at least one path with delay l' exists, then $\tilde{b}[l'] = 1$, otherwise $\tilde{b}[l'] = 0$.

For data detection, similar to (9), we rewrite (3) as

$$y[k,l] = \sum_{l'=0}^{l_\tau} \tilde{b}[l'] \sum_{k'=0}^{N-1} \tilde{h}[k', l']x_d[[k-k_{i'}]_N, \ [l-l']_M] + v[k,l] \quad (10)$$

for $k \in [0, N-1]$ and $l \notin [l_p, l_p + l_\tau]$. Now we can adapt the MP algorithm in [4] for data detection in (10).

Note that, to guarantee no interference between the received symbols for channel estimation and data detection, the guard symbols need to expand over a wider range over the Doppler axis, when compared to the integer Doppler case.

2) The Case of Reduced Guard Symbols: Employing full guard symbols to avoid interference provides more accurate channel estimation at the expense of reduced spectral efficiency. To improve the spectral efficiency, we can reduce the number of guard symbols and thus increase the number of data symbols, as discussed below.

We arrange the symbols as in Fig. 4a

$$x[k,l] = \begin{cases} x_p & k = k_p, l = l_p, \\ 0 & k_p - 2k_\nu - 2\hat{k} \le k \le k_p + 2k_\nu + 2\hat{k}, \\ & l_p - l_\tau \le l \le l_p + l_\tau, \\ x_d[k,l] & \text{otherwise} \end{cases}$$

for some integer $\hat{k}$. We can see that as the value of $\hat{k}$ reduces, the required number of guard symbols reduces, resulting in an increased spectral efficiency.

The received symbols $y[k,l], k_p - k_\nu - \hat{k} \le k \le k_p + k_\nu + \hat{k}, l_p \le l \le l_p + l_\tau$ are used for channel estimation, while the remaining $y[k,l]$ are used for data detection (see Fig. 4b)

From (3), for channel estimation, we have

$$y[k,l] = \tilde{b}[l-l_p]\tilde{h}[[k-k_p]_N, l-l_p]x_p + \mathcal{I}[k,l] + v[k,l] \quad (11)$$

for $k_p - k_\nu - \hat{k} \le k \le k_p + k_\nu + \hat{k}, l_p \le l \le l_p + l_\tau$. The second term $\mathcal{I}[k,l]$ is the interference from all neighboring data symbols $x_d[k,l]$, i.e.,

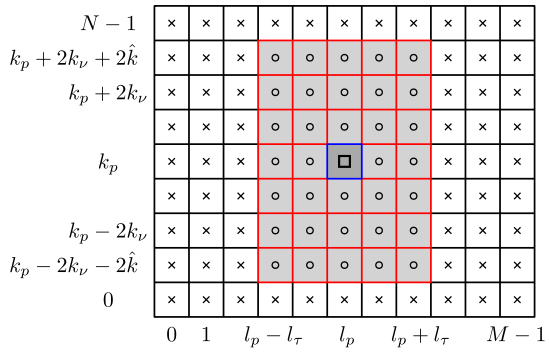

(a) Tx symbol arrangement (□: pilot; ○: guard symbols; ×: data symbols)

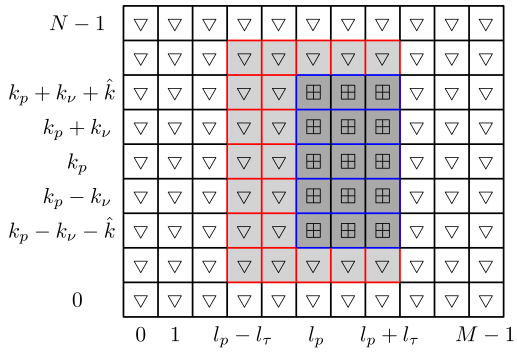

(b) Rx symbol pattern (▽: data detection, ⊞: channel estimation)

Fig. 4. The fractional Doppler case: Reduced guard symbols.

$$\mathcal{I}[k,l] = \sum_{k'=-k_\nu}^{k_\nu} \sum_{l'=0}^{l_\tau} b[k',l'] \sum_{q\notin[k_p-2k_\nu-2\hat{k},k_p+2k_\nu+2\hat{k}]} \bar{h}[k',l',\kappa',q]\, x_d\left[[k-k'+q]_N,[l-l']_M\right] \tag{12}$$

We observe that the interference $\mathcal{I}[k,l]$ gets larger for smaller $\hat{k}$, and similarly for the interference from pilot symbols to the received symbols for data detection.

Similar to the case of full guard symbols, we develop a threshold-based algorithm to estimate $\tilde{b}[l-l_p]$ and $\tilde{h}[[k-k_p]_N, l-l_p]$ based on (11) by treating $\mathcal{I}[k,l]$ as additive noise. Based on the simulation results (see next section), we demonstrate that the performance gap of the full guard symbols case (8% overhead) and reduced guard symbols case (2% overhead) is indeed marginal.

C. OTFS With Rectangular Waveforms

So far, we have assumed ideal transmit $g_{\text{tx}}(t)$ and receive $g_{\text{rx}}(t)$ pulses. Since the ideal pulses cannot be realized in practice, we now investigate OTFS with the more practical rectangular pulses at both transmitter and receiver. Although these pulses do not satisfy the bi-orthogonality conditions [5], we show that the proposed embedded channel estimation schemes can also be employed for this case.

Consider the integer Doppler case for simplicity. With rectangular pulses, the input-output symbol relationship can be rewritten as [5, Eq. (24)]

$$y[k,l] = \sum_{k'=-k_\nu}^{k_\nu} \sum_{l'=0}^{l_\tau} b[k',l']\hat{h}[k',l']\beta[k,l]x[[k-k']_N, [l-l']_M] + v[k,l]$$

where

$$\beta[k,l] = \begin{cases} e^{j2\pi\left(\frac{l-l'}{M}\right)\frac{k'}{N}} & l' \le l < M \\ \frac{N-1}{N} e^{j2\pi\left(\frac{l-l'}{M}\right)\frac{k'}{N}} e^{-j2\pi\left(\frac{[k-k']_N}{N}\right)} & 0 \le l < l'. \end{cases}$$

Hence, the threshold-based channel estimation technique can be straightforwardly employed by introducing a known phase $\beta[k,l]$ in the detection process. The thresholds for the rectangular waveforms remain the same as the ideal waveforms, since the channel differs only by a phase.

IV. Numerical Results

We illustrate the performance in terms of bit-error-rate (BER) of the uncoded OTFS using the proposed channel estimation schemes for integer and fractional Doppler cases. We adopt the following system parameters: Carrier frequency of 4 GHz, sub-carrier spacing of 15 KHz, $M = 512$, $N = 128$, and 4-QAM signaling. We recall that $\text{SNR}_p = |x_p|^2/\sigma^2$ and $\text{SNR}_d = \mathbb{E}(|x_d|^2)/\sigma^2$ to represent the average pilot and data SNRs, respectively. We use $\sigma_p^2 = 1/\text{SNR}_p$ to denote the effective noise power of the pilot signal. For simplicity, we assume $\sigma^2 = 1$ in all the simulations. For both OTFS and OFDM systems, Extended Vehicular A model [19] is used, and each delay tap has a single Doppler shift generated by using Jakes' formula, i.e., $\nu_i = \nu_{\max}\cos(\theta_i)$, where $\nu_{\max}$ is the maximum Doppler shift determined by the UE speed and θ_i is uniformly distributed over $[-\pi, \pi]$.

Fig. 5 shows a particular realization of the delay–Doppler channel grid for LTE EVA channel model with maximum UE speed 120 Kmph (i.e., $k_\nu = 4$). We see that there are few multipaths in the channel with most of them having Dopplers around -4 or 4.

A. The Integer Doppler Case

Fig. 6 compares BER versus data SNRs (SNR_d) for OTFS with known channel information (ideal case) and OTFS using the proposed channel estimation for the integer Doppler case with $\text{SNR}_p = 30$, 35, and 40 dB and $\mathcal{T} = 3\sigma_p$. We assume a delay–Doppler channel with maximum delay tap $l_\tau = 20$ and Doppler tap $k_\nu = 4$, which corresponds to maximum Doppler speed of 120 Kmph. The overhead for pilot and guard symbols is approximately 1% of an OTFS frame. We observe that the BER reduces as SNR_p increases, providing more accurate channel estimation and better data detection. Moreover, the performance

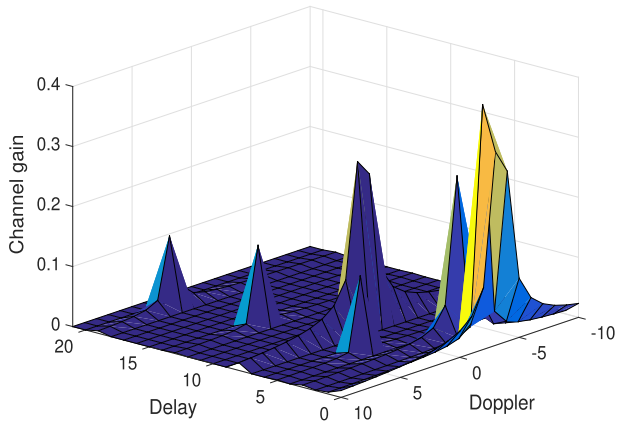

Fig. 5. Typical delay-Doppler channel response for LTE Extended Vehicular A channel model with maximum UE speed 120 Kmph.

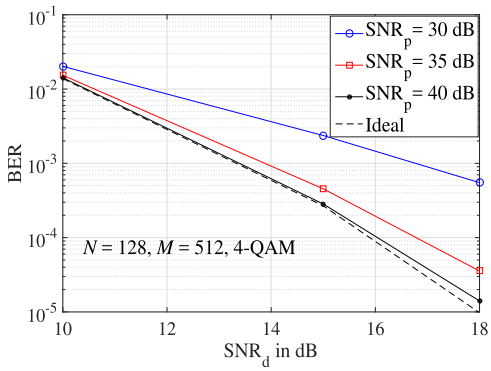

Fig. 6. BER versus SNR_d: Integer Doppler case.

TABLE I
MAXIMUM PEAK-TO-AVERAGE POWER RATIO OF OTFS FOR DIFFERENT PILOT POWERS WITH $M = 512$, $N = 128$, 120 Kmph, AND $\mathrm{SNR}_d = 18$ dB

System	Pilot power	MPAPR in dB
OTFS	18 dB	20.5258 dB
OTFS	30 dB	20.7386 dB
OTFS	40 dB	21.3253 dB
OTFS	50 dB	22.9563 dB
OFDM	-	27.0927 dB

of OTFS with channel estimation is very close to the ideal case, when $\mathrm{SNR}_p = 40$ dB (at least 20 dB higher than the data SNR_d).

Table I shows the maximum peak-to-average power ratio (MPAPR) of OTFS for different pilot powers with $M = 512$, $N = 128$, 120 Kmph, and $\mathrm{SNR}_d = 18$ dB. We observe that as the pilot power in OTFS is increasing, there is only a slight increase in MPAPR. This is due to the fact that OTFS spreads each delay–Doppler symbol in the entire time–frequency plane thanks to the ISFFT operation. Moreover, OTFS experiences 4 dB lower MPAPR compared to OFDM, which is due to the FFT operation across the time dimension (i.e., N point FFT) rather than the frequency dimension (i.e., M point FFT) in OFDM [7], [13].

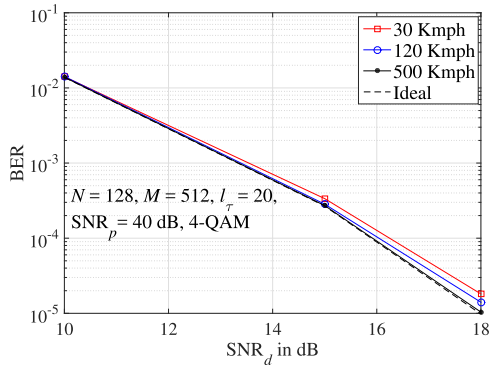

Fig. 7. BER versus SNR_d for different Dopplers.

TABLE II
CHANNEL ESTIMATION OVERHEAD FOR DIFFERENT SPEEDS

UE speeds	Pilot + Guard symbols	Data symbols	Channel estimation overhead
30 Kmph	205	65331	0.3%
120 Kmph	697	64839	1%
500 Kmph	2665	62871	4%

In Fig. 7, we perform comparisons of BER versus SNR_d for different Doppler frequencies with $\mathrm{SNR}_p = 40$ dB, $l_\tau = 20$, $\mathcal{T} = 3\sigma_p$, and 4-QAM. Consider UE speeds of 30, 120, and 500 Kmph corresponding to maximum Doppler tap $k_\nu = 1, 4$, and 16, respectively. Table II shows the number of pilot + guard symbols, data symbols, and overall channel estimation overhead used for different UE speeds. From the Fig. 7, we observe that the proposed estimation scheme exhibits highly similar performance under different Doppler frequencies except a slight performance improvement under higher Doppler frequencies (i.e., $k_\nu = 16$). This is due to the fact that more guard symbols and less data symbols are transmitted at high Doppler frequencies (see Table II), leading to better data detection capability at higher SNR_d. Please note that the pilot and guard symbols overhead is independent of the pilot and data SNR and it depends only on the maximum delay and Doppler of the channel. Since OTFS performs similarly at different frequencies, in the following, we consider only the UE speed of 120 kmph.

We next investigate the effect of the channel estimation threshold $\mathcal{T}$ on the system performance. Fix $\mathrm{SNR}_p = 40$ dB. Fig. 8 displays BER versus SNR_d with different $\mathcal{T}$. We observe that the BER performance improves as $\mathcal{T}$ increases. For small threshold values, the path false detection probability is higher (i.e., it is more likely to detect non-existent paths), which degrades the BER performance. However, at the same time, increasing the threshold beyond a certain value may cause the likely miss detection of paths with small path-gains, resulting in performance loss. Hence, there is an optimal threshold to balance the false detection and miss detection probabilities. For the given system parameters, we observe that the optimal threshold is approximately 3σ.

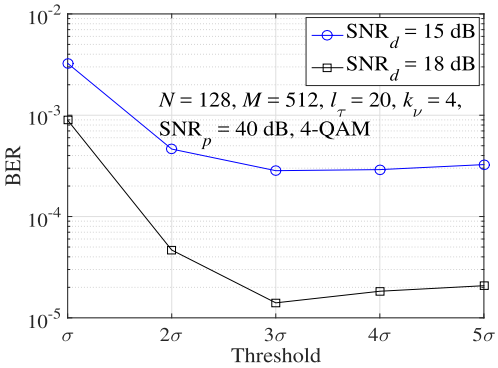

Fig. 8. BER versus channel estimation thresholds: Integer Doppler case.

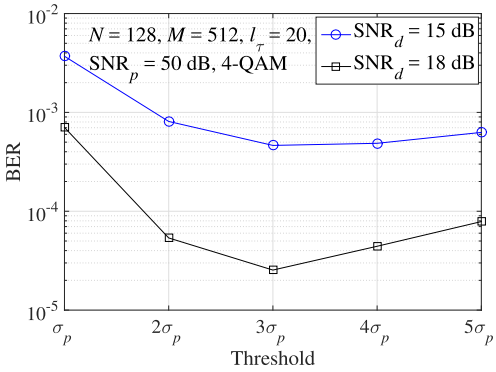

Fig. 10. BER versus channel estimation thresholds: Fractional Doppler with full guard symbols.

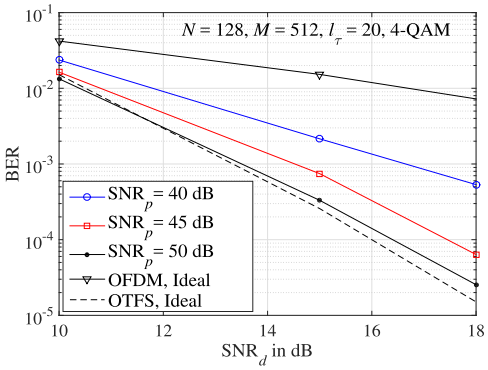

Fig. 9. BER versus SNR_d: Fractional Doppler with full guard symbols.

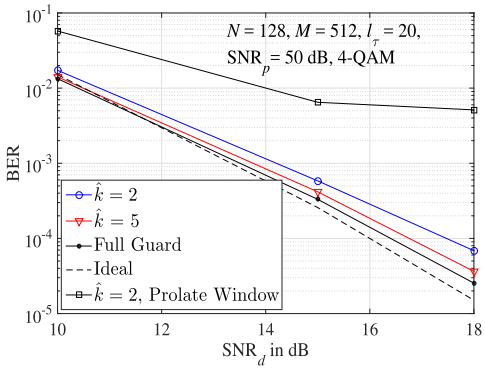

Fig. 11. BER versus SNR_d: Fractional Doppler with reduced guard symbols.

B. The Fractional Doppler Case

Fig. 9 shows the BER for different SNR_p with a threshold of $\mathcal{T} = 3\sigma_p$. In this case, the pilot and guard symbols occupy approximately 8% of an OTFS frame. Similar to the integer Doppler case, as the pilot power is increased, the error performance is improved. As $\mathrm{SNR}_p = 50$ dB, OTFS with our proposed embedded channel estimation attains similar performance as OTFS with known channel information. We can see that a larger pilot power is required for channels with fractional Doppler shifts than integer Doppler shifts. Last, we compare the BERs of OTFS with channel estimation and OFDM with known channel information and find that OTFS significantly outperforms OFDM, demonstrating the effectiveness of OTFS over delay–Doppler channels. Fig. 10 shows the BER versus the different thresholds ($\mathcal{T}$) for the fractional Doppler with full guard symbols case. It can be observed that the BER performance is similar to the integer Doppler case with the optimal threshold as $3\sigma_p$.

In Fig. 11, we compare the BER performance of OTFS using the proposed channel estimation scheme with reduced guard symbols for $\hat{k} = 2$ and 5. Here, for $\hat{k} = 2$, we also apply a discrete prolate spheroidal window (time half bandwidth product is one) at the receiver. The proposed channel estimation and MP detector is also applied for the prolate window. Fix $\mathrm{SNR}_p = 50$ dB, $\mathcal{T} = 3\sigma_p$, and 4-QAM. With $\hat{k} = 2$, and 5, the overheads for pilot and guard symbols are roughly 1.5% and 2.3%, respectively, which are much less than the full guard symbols case (roughly 8%). We observe that, as $\hat{k}$ becomes larger, the performance improves. In particular, with $\hat{k} = 5$, the performance is very close to that with full guard symbols. For larger $\hat{k}$, smaller interference from neighboring data symbols improves the channel estimation accuracy. Hence, there is a tradeoff between spectral efficiency and error performance.

Further, we can see that the OTFS with rectangular window performs better than that with prolate window due to the noise correlations caused by the prolate window (see II-C). A better detection scheme that can handle the noise correlations will be considered in future work.

In Fig. 12, we illustrate the effectiveness of the proposed channel estimation scheme with full and reduced guard symbols, respectively, using 16-QAM, $\mathrm{SNR}_p = 60$ dB, and $\mathcal{T} = 3\sigma_p$. We see that with the higher pilot power (i.e., 60 dB), the performance of our channel estimation scheme with full guard symbols is the same as that of the ideal case. Moreover, with 16-QAM, a larger number of guard symbols are required (i.e., $\hat{k} = 10$, about 3.6% guard symbols overhead) to achieve a performance close to the full guard symbols case, when compared to the 4-QAM case that adopts $\hat{k} = 5$, about 2.3% guard symbols overhead. This is due to the fact that the data detection of 16-QAM case is more sensitive to the channel estimation and hence requires more guard symbols.

Fig. 13 shows the BER performance comparison between OTFS and OFDM. In particular,

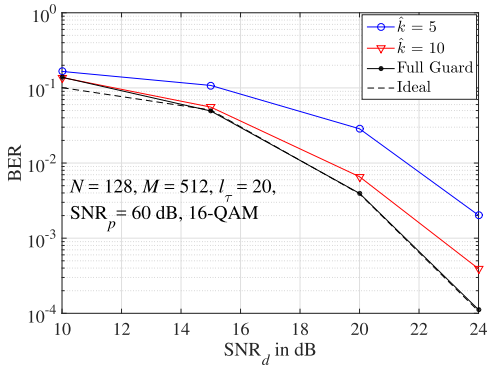

Fig. 12. BER versus SNR_d: Fractional Doppler with reduced guard symbols for 16-QAM.

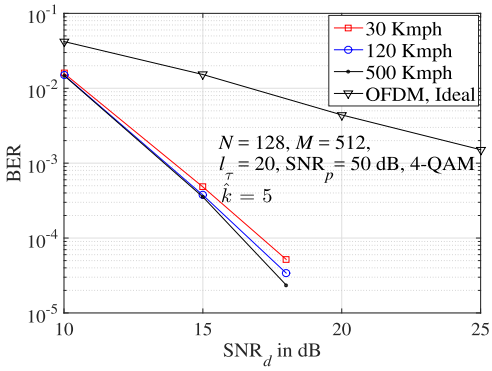

Fig. 13. BER versus SNR_d for different Dopplers with rectangular waveforms.

- for OTFS, we employ the proposed channel estimation with MP algorithm using practically realizable rectangular waveforms under different UE speeds;
- for OFDM, we assume the ideal channel information with known inter carrier interference (ICI) channel coefficients with 30 Kmph UE speed, and use the MP detection algorithm proposed in [5] that can efficiently cancel ICI.

We have the following key observations:

1) OTFS with realistic rectangular waveforms performs similarly with different Dopplers (30, 120, 500 Kmphs) and significantly outperforms OFDM with ideal channel information defined over the same numerology (subcarrier spacing, CP, M, and N). Hence, we can summarize the main advantages of OTFS for different Dopplers as:
   - using the same pilot structure and similar small pilot overhead.
   - having the same channel estimation and detection complexity for different Dopplers.
   - enjoying the same BER performance for different Dopplers.

   These benefits are contrasted with the case of OFDM which suffers ICI causing performance degradation.
2) OTFS with *non-ideal* channel estimation outperforms OFDM with *ideal* channel information with known ICI channel coefficients. Note that in practice, it is also very difficult to obtain ICI channel coefficients in OFDM. This requires large pilot overhead and high complexity channel estimation procedures. Alternatively, equalizing the ICI channel coefficients in OFDM can be avoided by passive method of increasing the sub-carrier spacing which, in turns reduces proportionally the symbol time hence adds to the CP overhead resulting in lower spectral efficiency.
3) We did not include the BER performance of OFDM with *non-ideal* LTE time-frequency channel estimation since it is certainly worse than that of OFDM with ideal channel information. Moreover, in practice, OFDM with LTE time-frequency channel estimation is highly complex as it involves selecting many parameters and is highly dependent on the channel interpolation algorithms.

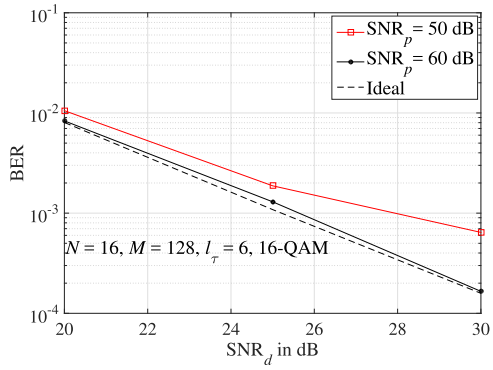

Fig. 14. BER versus SNR_d: Low latency communication.

C. OTFS Under Low Latency Communications

As next-generation wireless communications mostly require low latency communications, we next simulate the proposed OTFS channel estimation schemes under such scenario. Fig. 14 shows the OTFS performance for low latency application with $N=16$ and $M=128$, corresponding to frame duration of 1.1 ms. We consider a UE speed of 120 Kmph, corresponding to a maximum Doppler tap, $k_\nu=1$. We consider the channel estimation scheme with full guard symbols as the reduced guard symbols case will not improve significantly the spectral efficiency with small N. We observe that the OTFS performance with channel estimation is very close to the ideal case with $\text{SNR}_p=60$ dB. Hence, we can conclude that the proposed channel estimation schemes are very efficient under low latency communications.

V. Extensions to MIMO and Multiuser Uplink/Downlink

In this section, we extend our embedded channel estimation for point-to-point SISO OTFS systems to MIMO and multi-user uplink/downlink, respectively.

A. Point-to-Point MIMO

In a MIMO system, each transmit (Tx) antenna arranges its own pilot, guard, and information symbols on the delay–Doppler grid for transmission (see Fig. 15). The pilot symbol is used to estimate the channels from that Tx antenna to each receive

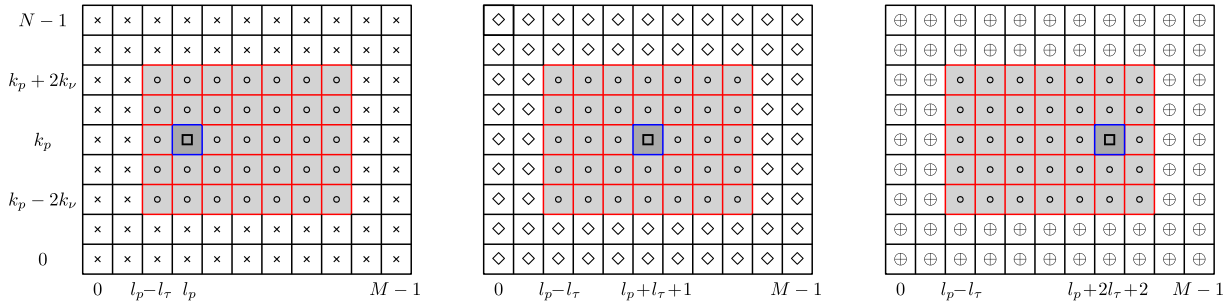

(a) Antenna 1 (×: antenna 1 data symbol) (b) Antenna 2 (◇: antenna 2 data symbol) (c) Antenna 3 (⊕: antenna 3 data symbol)

Fig. 15. Tx pilot, guard, and data symbols for MIMO OTFS system (□: pilot; ○: guard symbols).

(Rx) antenna. At each Rx antenna, different groups of received symbols are used for channel estimation from that Rx antenna to the Tx antennas, and for data detection from the Tx antennas. Moreover, the received symbols for data detection of the Rx antennas are jointly decoded using MP algorithm. The symbol arrangements from the Tx antennas have to be carefully designed to facilitate the channel estimation and data detection at the Rx antennas. In the following, we describe one such arrangement.

Consider a MIMO system with arbitrary $N_t \geq 1$ and $N_r \geq 1$. For ease of presentation, we consider channels with integer Doppler shifts and the case of fractional Doppler shifts is a straightforward extension. Inspired by our previous study in Section III, we propose the following symbol arrangement $x^{n_t}[k,l]$ for the n_t-th Tx antenna ($n_t = 1, \ldots, N_t$)

$$x^{n_t}[k,l] = \begin{cases} x_p & k = k_p, l = l_p + (n_t-1)(l_\tau+1), \\ 0 & k_p - 2k_\nu \leq k \leq k_p + 2k_\nu, \\ & l_p - l_\tau \leq l \leq l_p + N_t l_\tau + N_t - 1, \\ x_d^{n_t}[k,l] & \text{otherwise} \end{cases}$$

where $x_d^{n_t}[k,l]$ denotes the data symbol at location $[k,l]$ of n_t-th Tx antenna. We can see that the pilot symbols of the Tx antennas are sufficiently separated (by the maximum delay tap l_τ along the delay axis) so that they do not interfere with each other at the Rx antennas, as demonstrated in Fig. 15 for an exemplary MIMO system with three Tx antennas.

At the n_r-th Rx antenna ($n_r = 1, \ldots, N_r$), the received symbols $y^{n_r}[k,l], k_p - k_\nu \leq k \leq k_p + k_\nu, l_p + (n_t-1)(l_\tau + 1) \leq l \leq l_p + n_t l_\tau + n_t - 1$, are used for channel estimation to the n_t-th Tx antenna. These received symbols are affected by the pilot signal of the n_t-th Tx antenna and by the channel between the n_t-th Tx and n_r-th Rx antennas only, as shown in Fig. 16. Hence, the channel estimation technique in Section III can be applied straightforwardly. The remaining received symbols of the n_r-th Rx antenna are functions of the data symbols from all the Tx antennas and thus a joint detection in [12] can be applied. We omit the details for brevity.

B. Multiuser

Consider a multiuser system, where single-antenna users communicate with base station in uplink or downlink. The base station has either single or multiple antennas. In the following, we present embedded channel estimation schemes using Tx symbol arrangement for the users and base station.

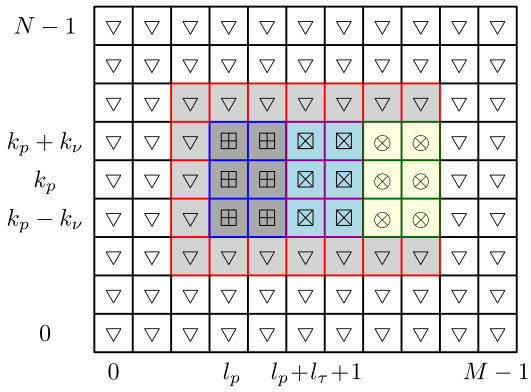

Fig. 16. Rx symbol pattern at one antenna of MIMO OTFS system (▽: data detection, ⊞, ⊠, ⊗: channel estimation for Tx antenna 1, 2, and 3, respectively).

1) Uplink: Consider single-antenna base station. We assume orthogonal resource allocation among the users.

One example of the Tx symbol arrangements for three-user case is shown in Fig. 17. For each user, in each OTFS frame, the grid locations $[k,l], k_p - 2k_\nu \leq k \leq k_p + 2k_\nu, l_p - l_\tau \leq l \leq l_p + N_u l_\tau + N_u - 1$ are used for pilot and guard symbols, where N_u is the number of users. The pilot symbols of the users are located sufficiently apart at suitable locations as in the MIMO case. Moreover, each user occupies only a non-overlapping portion of the rest of the grid locations for its data transmissions. Zero guard symbols are placed between different users data symbols to ensure orthogonal resource allocations. Fig. 17 shows the pilot, guard, and data symbols arrangement for 3 users, where green, blue, and yellow grids contains data for Users 1, 2, and 3, respectively. The data portion for each user depends on the resource requirement/allocation. Based on the Tx symbol arrangements, the base station exploits suitable received symbols for channel estimation and data detection for the users.

2) Downlink: Consider single-antenna base station, transmitting a pilot symbol being enclosed with guard symbols, similar to the point-to-point SISO case. This pilot signal is used by all the users to estimate the channel from itself to the base station. The rest of delay–Doppler grid locations is used for data

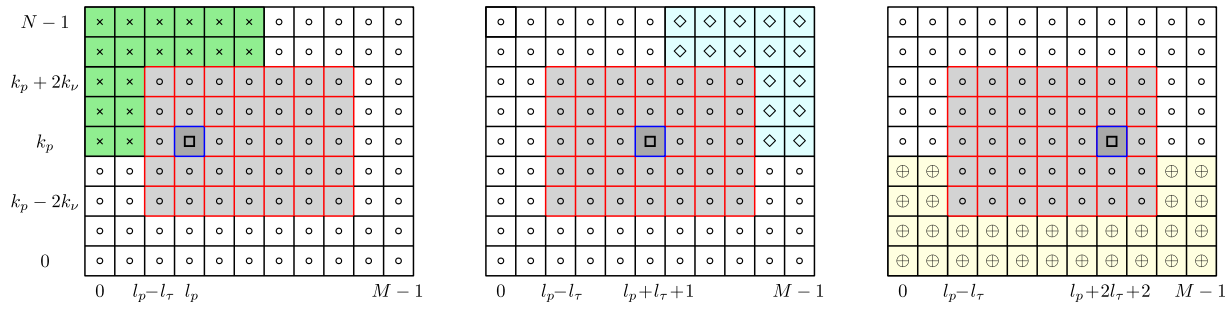

(a) User 1 (×: user 1 data symbol) (b) User 2 (◇: user 2 data symbol) (c) User 3 (⊕: user 3 data symbol)

Fig. 17. Tx pilot, guard, and data symbols for multiuser uplink OTFS system (□: pilot; ○: guard symbols).

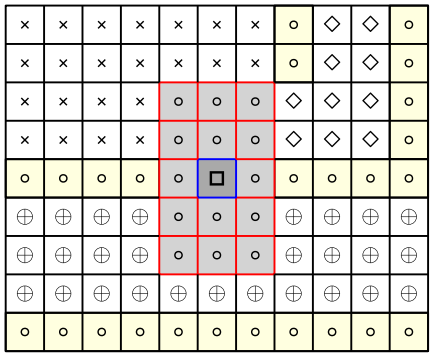

Fig. 18. Tx pilot and data arrangement for multiuser downlink OTFS system (□: pilot; ○: guard symbols; ×, ◇, ⊕: data symbols for users 1, 2, and 3, respectively).

TABLE III
TOTAL NUMBER OF PILOT AND GUARD SYMBOLS REQUIRED FOR DIFFERENT EMBEDDED CHANNEL ESTIMATION SCHEMES

Method	Pilot + guard symbols
SISO - integer Doppler	$(2l_\tau+1)(4k_\nu+1)$
SISO - fractional Doppler full guard symbols	$(2l_\tau+1)(N)$
SISO - fractional Doppler reduced guard symbols	$(2l_\tau+1)\left(4(k_\nu+\hat{k})+1\right)$
MIMO - N_t transmit antennas	$((N_t+1)l_\tau+N_t)\left(4(k_\nu+\hat{k})+1\right)$
Multiuser uplink - N_u users with 1 antenna	$((N_u+1)l_\tau+N_u)\left(4(k_\nu+\hat{k})+1\right)$
Multiuser downlink - base station with 1 antenna	$(2l_\tau+1)\left(4(k_\nu+\hat{k})+1\right)$

transmissions to the users. Since orthogonal resource allocation is required, data symbols for users should be sufficiently separated using guard symbols to avoid inter-user interference, as shown in Fig. 18, where yellow grids represent the guard symbols between users. Each user exploits appropriate groups of received symbols for channel estimation and detection of its own data.

Table III summarizes the total number of pilot and guard symbols required for the different channel estimation methods in our paper.

VI. CONCLUSION

In this work, we have developed embedded pilot-aided OTFS channel estimation schemes. In particular, we arrange pilot, guard, and information symbols in the delay–Doppler grids to suitably avoid interference between pilot and data symbols. We design such arrangements for OTFS with ideal and rectangular pulses over channels with integer or fractional Doppler paths, respectively. At the receiver, channel estimation is performed based on a threshold method and the estimated channel information is used for data detection via a MP algorithm. We compare by simulations the error performance of OTFS using the proposed channel estimation schemes and OTFS with perfectly known channel information and observe only a marginal performance loss. Further, we show that OTFS with our channel estimation significantly outperforms OFDM with ideal channel information. Extensions of the proposed schemes to MIMO and multi-user uplink/downlink have been presented.

ACKNOWLEDGMENT

Simulations were undertaken with the assistance of resources and services from the National Computational Infrastructure (NCI), which is supported by the Australian Government.

REFERENCES

[1] R. Hadani *et al.*, "Orthogonal time frequency space modulation," in *Proc. IEEE WCNC*, San Francisco, CA, USA, Mar. 2017.
[2] R. Hadani *et al.*, "Orthogonal time frequency space modulation," in *Proc. IEEE Wireless Commun. Netw. Conf. (WCNC)*, San Francisco, CA, USA, 2017, pp. 1–6.
[3] R. Hadani and A. Monk, "OTFS: A new generation of modulation addressing the challenges of 5G," Santa Clara, CA 95051, USA: OTFS Physics White Paper, Cohere Technologies, Feb. 7, 2018. [Online]. Available: https://arxiv.org/pdf/1802.02623.pdf
[4] P. Raviteja, K. T. Phan, Q. Jin, Y. Hong, and E. Viterbo, "Low-complexity iterative detection for orthogonal time frequency space modulation," in *Proc. IEEE WCNC*, Barcelona, Spain, Apr. 2018, pp. 1–6.
[5] P. Raviteja, K. T. Phan, Y. Hong, and E. Viterbo, "Interference cancellation and iterative detection for orthogonal time frequency space modulation," *IEEE Trans. Wireless Commun.*, vol. 17, no. 10, pp. 6501–6515, Oct. 2018.
[6] P. Raviteja, K. T. Phan, Y. Hong, and E. Viterbo, "Embedded delay-Doppler channel estimation for orthogonal time frequency space modulation," in *Proc. IEEE VTC2018-fall*, Chicago, IL, USA, Aug. 2018, pp. 1–6.
[7] P. Raviteja, Y. Hong, E. Viterbo, and E. Biglieri, "Practical pulse-shaping waveforms for reduced-cyclic-prefix OTFS," *IEEE Trans. Veh. Technol.*, vol. 68, no. 1, pp. 957–961, Jan. 2019.

[8] L. Li *et al.*, "A simple two-stage equalizer with simplified orthogonal time frequency space modulation over rapidly time-varying channels," Sep. 2017. [Online]. Available: https://arxiv.org/abs/1709.02505
[9] T. Zemen, M. Hofer, and D. Loeschenbrand, "Low-complexity equalization for orthogonal time and frequency signaling (OTFS)," Oct. 2017. [Online]. Available: https://arxiv.org/pdf/1710.09916.pdf
[10] T. Zemen, M. Hofer, D. Loeschenbrand, and C. Pacher, "Iterative detection for orthogonal precoding in doubly selective channels," in *Proc. 2018 IEEE 29th Annu. Int. Symp. Personal, Indoor and Mobile Radio Commun. (PIMRC)*, 2018.
[11] K. R. Murali and A. Chockalingam, "On OTFS modulation for high-Doppler fading channels," in *Proc. ITA'*, San Diego, CA, USA, Feb. 2018, pp. 1–10.
[12] M. K. Ramachandran and A. Chockalingam, "MIMO-OTFS in high-Doppler fading channels: Signal detection and channel estimation," in *Proc. 2018 IEEE Global Commun. Conf. (GLOBECOM)*, 2018.
[13] A. Farhang, A. Rezazadeh, R. L. E. Doyle, and B. Farhang-Boroujeny, "Low complexity modem structure for OFDM-based orthogonal time frequency space modulation," *IEEE Wireless Commun. Lett.*, vol. 7, no. 3, pp. 344–347, Jun. 2018.
[14] A. Rezazadeh, R. A. Farhang, M. Ji, R. R. Chen, and B. Farhang-Boroujeny, "Analysis of discrete-time MIMO OFDM-based orthogonal time frequency space modulation," in *Proc. IEEE ICC*, Kansas City, MO, USA, 2018, pp. 1–6.
[15] R. Hadani and S. Rakib., "OTFS methods of data channel characterization and uses thereof," U.S. Patent 9 444 514 B2, Sep. 13, 2016.
[16] A. Fish, S. Gurevich, R. Hadani, A. M. Sayeed, and O. Schwartz, "Delay-Doppler channel estimation in almost linear complexity," *IEEE Trans. Inf. Theory*, vol. 59, no. 11, pp. 7632–7644, Nov. 2013.
[17] A. Monk, R. Hadani, M. Tsatsanis, and S. Rakib, "OTFS - Orthogonal time frequency space: A novel modulation technique meeting 5G high mobility and massive MIMO challenges," 2016. Available online: https://arxiv.org/abs/1608.02993
[18] W. C Jakes, Jr., *Microwave Mobile Communications.* New York, NY, USA: Wiley, 1974.
[19] "LTE; "Evolved Universal Terrestrial Radio Access (E-UTRA); Base Station (BS) radio transmission and reception," 3GPP TS 36.104 version 8.6. 0 Release 8, Jul. 2009," ETSI TS.
[20] D. N. C. Tse and P. Viswanath, *Fundamentals of Wireless Communications.* Cambridge, U.K.: Cambridge Univ. Press, 2005.

P. Raviteja (S'15) received the B.Tech degree in electronics and communication from Jawaharlal Nehru Technological University, Hyderabad, India in 2012. He completed M.E. degree in telecommunications from the Indian Institute of Science, Bangalore, India in 2014. He is currently pursuing the Ph.D. degree with the Department of Electrical and Computer Systems Engineering, Monash University, Australia. From 2014 to 2015, he was at Qualcomm India Private Limited, Bangalore, working on WLAN systems design. His current research interests include new waveform designs for next generation wireless systems. Dr. Raviteja was a recipient of Prof. S. V. C. Aiya Medal from the Indian Institute of Science in 2014.

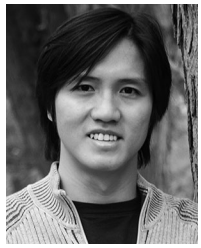

Khoa T. Phan (M'17) received the B. Eng. degree in telecommunications (first class honours) from the University of New South Wales (UNSW), Sydney, NSW, Australia, in 2006, the M.Sc. degrees in electrical engineering from the University of Alberta, Edmonton, AB, Canada, in 2008, and California Institute of Technology (Caltech), Pasadena, CA, USA, in 2009, respectively, and the Ph.D. degree in Electrical Engineering from McGill University, Montreal, QC, Canada in 2017. He was a Researcher at the Electrical Engineering Department, University of California, Los Angeles (UCLA), Los Angeles, CA, USA, from 2009 to 2011. From January 2017 to July 2018, he was a Research Fellow in the Electrical and Computer Systems Engineering Department at Monash University, Clayton, VIC, Australia. He is currently a Lecturer in the Department of Computer Science and Information Technology, School of Engineering and Mathematical Sciences, La Trobe University, Bendigo, VIC, Australia. His research interests are broadly design, control, and optimisation of 5G mobile communications networks with applications in the Internet of Things (IoT), machine-type communications (MTC), smart grids, and cloud computing.

Dr. Phan has been awarded several prestigious fellowships including the Australian Development Scholarship (UNSW), the Alberta Ingenuity Fund Student Fellowship and the iCORE Graduate Student Award (Alberta), the Atwood Fellowship (Caltech), the McGill Doctoral Engineering Award, and the SRTelecom Doctoral Award (McGill).

Yi Hong (S'00–M'05–SM'10) received the Ph.D. degree in electrical engineering and telecommunications from the University of New South Wales (UNSW), Sydney.

She was an Associate Editor for IEEE WIRELESS COMMUNICATION LETTERS and TRANSACTIONS ON EMERGING TELECOMMUNICATIONS TECHNOLOGIES (ETT). She was the General Co-Chair of *IEEE Information Theory Workshop* 2014, Hobart; the Technical Program Committee Chair of *Australian Communications Theory Workshop* 2011, Melbourne; and the Publicity Chair at the *IEEE Information Theory Workshop* 2009, Sicily. She was a Technical Program Committee member for many IEEE leading conferences. She is currently a Senior Lecturer at the Department of Electrical and Computer Systems Eng., Monash University, Melbourne, Australia. She currently serves on the Australian Research Council College of Experts (2018–2020). Her research interests include communication theory, coding and information theory with applications to telecommunication engineering. Dr. Hong was the recipient of the *NICTA-ACoRN Earlier Career Researcher Award* at the *Australian Communication Theory Workshop*, Adelaide, Australia, 2007.